Estimates of antiproton production and annihilation in relativistic nucleus-nucleus collisions

B. Shiva Kumar, S.V. Greene, and J.T. Mitchell
Yale University, A.W. Wright Nuclear Structure Laboratory, New Haven, Connecticut 06520
(Received 9 May 1994)

We describe a simple model developed to study the production and annihilation of antiprotons in nucleus-nucleus collisions. The model can be used to calculate the antiproton yields as functions of global observables such as multiplicity, transverse energy, and zero degree energy. We discuss the predictions of the model, and its relevance to the antiproton measurements at the Brookhaven National Laboratory Alternating Gradient Synchrotron facility.

PACS number(s): 25.75.+r

I. INTRODUCTION

Nucleus-nucleus collisions at relativistic energies have been the subject of active theoretical and experimenal investigation as a means of creating and studying states of hot and dense nuclear and quark matter [1]. The studies have attempted to look for specific signatures for quark matter formation in events which have been characterized through measurement of global or impact parameter defining variables such as transverse energy E_t, charged particle multiplicity N_c, and zero degree energy E_{ZD}. Amongst the signatures proposed for the detection of a quark-gluon plasma is the enhanced production of antibaryons [2]. We describe herein a simple model to calculate the yields of antiprotons produced in nucleus-nucleus collisions as functions of impact parameter. The model attempts simultaneously to describe the antiproton ($\bar{p}$) yields, measurements of global variables, and their correlations.

The $\bar{p}$ has been suggested as a probe of the hot and dense hadronic matter being created in heavy ion collisions since it annihilates with large probability in baryon rich regions [3]. Several experiments at the Brookhaven Alternating Gradient Synchrotrotron (AGS) have measured the spectra of antiprotons [4–17]. A clear picture of how antiprotons are created or annihilated has not yet emerged for several reasons, including the simultaneous lack of complete kinematic coverage and centrality information, and insufficient statistics. Also, there have been theoretical studies of $\bar{p}$ production at AGS energies using the relativistic quantum molecular dynamics (RQMD) [18,19] and a relativistic cascade (ARC) [20–22] models. These models are rather sophisticated in their attempts to follow the space-time development of the nucleus-nucleus collision environment, and the production and annihilation of antiprotons. While RQMD is able to describe available data by relying on the enhanced production of antiprotons followed by the annihilation of a large fraction of the produced antiprotons, ARC describes the data by producing less antiprotons initially, but the annihilation of antiprotons is "screened" in the high density environment of the collision on account of collisions with mesons. We know from measurements [4–16] that typically, one $\bar{p}$ is produced in every 100 ^{28}Si+^{208}Pb nucleus-nucleus ($A + A$) collisions at a beam energy of 14.6A GeV. If one wants to describe such small yields while accounting for the small geometrical acceptances ($< 1\%$ of 4π) of the spectrometers used in the data collection, the computations require inordinate resources. Presently, systematic and statistical uncertainties in both the measurements and the calculations preclude a detailed quantitative understanding of $\bar{p}$ production. Until such time that better calculations and measurements become available, we can use simple models to understand qualitatively the several interesting features seen in the data. Such investigations will also allow us to explore the measurements that need to be made by future experiments, as is discussed below. It bears emphasis that we are trying to understand the shapes of global variable distributions and $\bar{p}$ distributions with a few simple assumptions and parameters. Some of this physics is not easily accessible via more sophisticated models such as ARC and RQMD. In this paper, we give a detailed description of our model and its results. These have been discussed briefly elsewhere [6,10].

II. GLOBAL VARIABLES

In order to describe the production and annihilation of antiprotons in nucleus-nucleus collisions we need to develop prescriptions for describing the collision, along with the production and subsequent annihilation of antiprotons. There are two classes of models that attempt to describe nucleus-nucleus collisions. The first class [23–28] traces the evolution of the individual nucleon-nucleon collisions. The consequences of interactions are modeled by various fragmentation schemes or measured experimental cross sections, conserving energy, baryon number, quark flavors, etc. The secondary or produced particles are propagated through the target, projectile, and spectator matter with or without further interaction. The second class of models [29–32] does not follow

 ©1994 The American Physical Society

the detailed evolution of the individual collisions. Instead, the desired distributions are parametrized based on proton+proton ($p + p$) and proton+nucleus ($p + A$) data. The $A + A$ distributions are then obtained as a convolution of $p + A$ distributions. We follow a hybrid approach. Individual projectile nucleons are propagated through the target, and the consequences of their interactions are parametrized, as will be described below. In particular, the model generates antiprotons, and propagates them through the target and projectile environments in order to ascertain whether they emerge therefrom without annihilation. While such a model does not, by construction, have a detailed treatment of the time dependent evolution of the nucleus-nucleus collisions, it allows us to appreciate some of the features seen in the data.

The E814 experiment has measured the mean multiplicity of beam rapidity nucleons surviving a collision without interaction, as functions of E_t, and N_c [33–36]. These data have been interpreted in terms of an in-medium nucleon-nucleon cross section. We have attempted to reproduce the features seen in these data using the calculation we describe below. The calculations are motivated by the following two observations. First, the amount of energy deposited by a projectile nucleus in a target nucleus is proportional to the number of projectile nucleons that have interacted. Second, the shapes of the $d\sigma/dE_t$ and $d\sigma/dN_c$ distributions are dominated by the geometry of the collision. In the calculation, individual nucleons in the projectile are transported through the target, which is assumed to be the same for all projectile nucleons (i.e., the target nucleons do not move). Interactions are Monte Carlo generated and depend on an inelastic interaction cross section of 29 mb, a number that is consistent with the E814 measurement. If a nucleon interacts, it contributes to the generation of transverse energy, and charged particle multiplicity. If a nucleon survives without interaction, it is treated as a projectilelike particle, and contributes to the mean multiplicity of leading baryons and to the zero degree energy. For nucleons that interact, we determine if projectile-target nucleon combinations are interacting for the first time, or if either one of these nucleons has interacted previously. These considerations become important in the discussion of antiprotons. The nucleus-nucleus interaction cross sections in our model are 1736 mb, 2297 mb, and 3644 mb, respectively, for Si + Al, Cu, and Pb collisions.

Figure 1 shows transverse energy and charged particle multiplicity measured by the E814 target calorimeter [34] and the silicon multiplicity detector [37], respectively. The model is able to describe these distributions rather well. In order to reproduce the measured data, the assumption was made that a certain multiplicity and transverse energy was produced by each projectile nucleon that had interacted with the target. Further, "rescattering" in the target was simulated by creating additional transverse energy or multiplicity if a struck projectile nucleon interacted far from the surface of the target nucleus. The extent of this increase was directly proportional to the distance R_s of the nucleon from the nuclear surface,

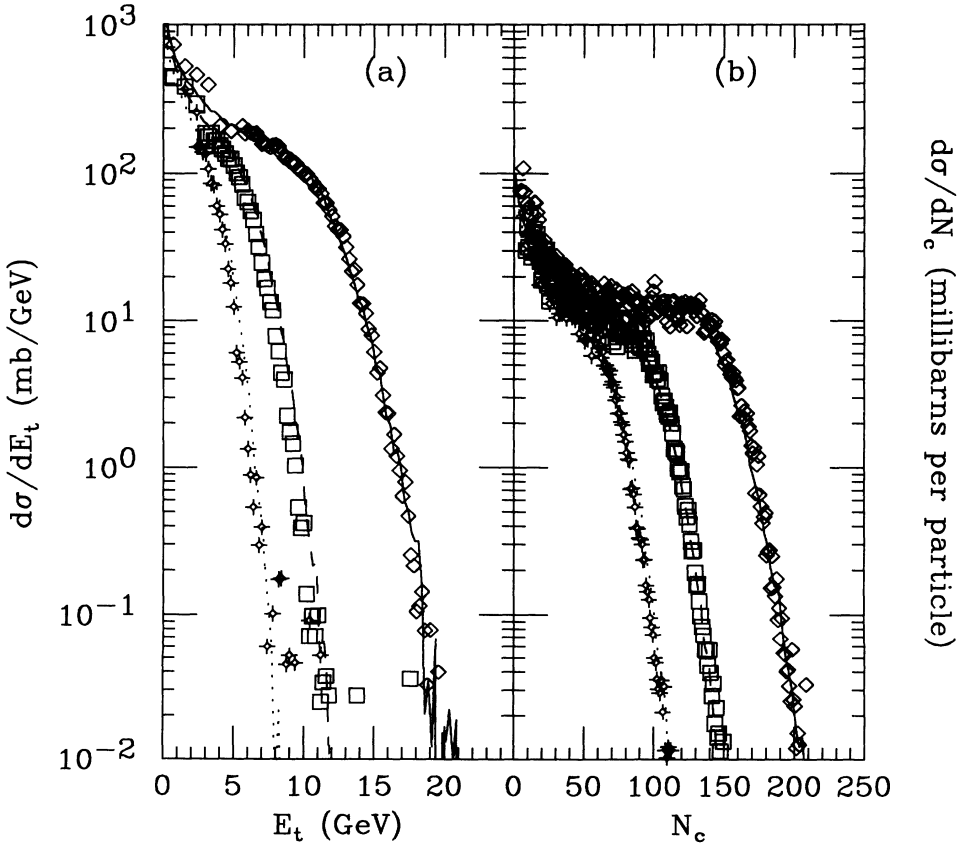

FIG. 1. Transverse energy distributions (left) and charged particle multiplicity distributions (right) measured by the E814 Collaboration for Si ions interacting with targets of Al, Cu, and Pb [34,37]. The predictions of our model are shown as curves.

in the direction of its motion. The equations below detail how, for each projectile nucleon i that interacts, the transverse energy E_t^i and multiplicity N_c^i are calculated:

$$E_t^i = f_g(\overline{E_t}, \sigma_{E_t})[1 + R_s R_{E_t}] , \quad (1)$$

$$N_c^i = f_g(\overline{N_c}, \sigma_{N_c})[1 + R_s R_{N_c}] , \quad (2)$$

where $\overline{E_t}$ and $\overline{N_c}$ are the mean, σ_{E_t} and σ_{N_c} are the standard deviations, and R_{E_t} and R_{N_c} are the rescattering factors, respectively, for the transverse energy and charged particle multiplicity produced per nucleon. The $f_g(a,b)$ are Monte Carlo generated values from Gaussian distributions of means a, and standard deviations b. The E_t and N_c for each nucleus-nucleus collision are then obtained as $E_t = \sum_i E_t^i$ and $N_c = \sum_i N_c^i$. The data in Fig. 1 cannot be described without the inclusion of rescattering, an effect which is ignored in previous calculations [29,30]. Table I lists the parameters used in our calculation. We emphasize that while our prescriptions are physics motivated, they are too simplistic to warrant detailed conclusions being drawn based on the magnitudes of the parameters (one each for the mean, standard deviation, and rescattering for the E_t and N_c produced by each interacted nucleon). The parameters depend on the geometrical acceptance of the detectors, and details of the response of the detectors to incident radiation. The parameters used to describe the data of the E802 experiment are related to the parameters chosen to describe the data from the E814 experiment by simple multiplicative factors. The quantities that are "averaged" over by changing the value of the rescattering parameters include the physics of the changes in the effective collision center of mass as a function of impact parameter, the differences in the geometrical acceptances, and the responses of the detectors to radiation. An important message from this exercise, however, is that the shapes of the E_t and N_c distributions are dominated by the nucleus-nucleus collision geometry. We are impressed by how well the distributions are described for all three targets over several orders of magnitude in cross section using only a few parameters.

TABLE I. The parameters used in the calculation of the global variable distributions (see text). The $p + A$ distributions for E_t^i and N_c^i are assumed to be Gaussian. The parameters for the E814 distributions (mean and standard deviation) can be multiplied by 1.8 (for the E_t distributions) and 2.5 (for the N_c distributions), respectively, to get the corresponding parameters that describe the E802 lead glass data, and TMA multiplicity distributions.

Parameter	E814	E802
$\overline{E_t}$	0.15	0.27
σ_{E_t}	0.13	0.234
R_{E_t}	0.75	0.70
$\overline{N_c}$	3.0	7.5
σ_{N_c}	2.0	5.0
R_{N_c}	0.3	1.25

For a model to be realistic, it should be able to describe simultaneously the E_t or N_c, and the E_{ZD} distributions. The E_{ZD} was calculated from the number of projectile nucleons that had not interacted. Each of these nucleons (at a beam energy of 14.6 GeV per nucleon) will deposit 13.6 GeV in a zero degree calorimeter. This energy, when measured, will be uncertain by the energy resolution of the calorimeter. Figure 2 is a plot of the correlation between the N_c and the E_{ZD} distributions measured by the E814 Collaboration [37]. The model calculations are shown as the curves, and are able to describe the trends seen in the data rather well. Again, it is important to note that the shapes of these correlations are dominated by the geometry of the collision, and the proper choice of the in-medium interaction cross section.

Figure 3 shows the distributions of energy measured by experiment E814 in a zero degree calorimeter. The preliminary data [6] are shown as dashed lines. The model calculations are shown as solid lines. The model is able to describe the data rather well, except for peripheral Si+Al collisions, where some of the disagreements can be attributed to experimental difficulties in the triggering of peripheral Si+Al collisions. The procedure to select interactions in the E814 experiment relied on the measurement of charged particle multiplicity, and was therefore susceptible to δ electrons.

The mean multiplicity of beam rapidity fragments is a measure of the interaction cross section of the projectile nucleons with the target. Figure 4 is a plot of the mean multiplicity of beam rapidity protons measured by the E814 experiment [34,36]. The curves are the predictions of our model under the assumption that the in-medium interaction cross section for nucleons is 29 mb. The model

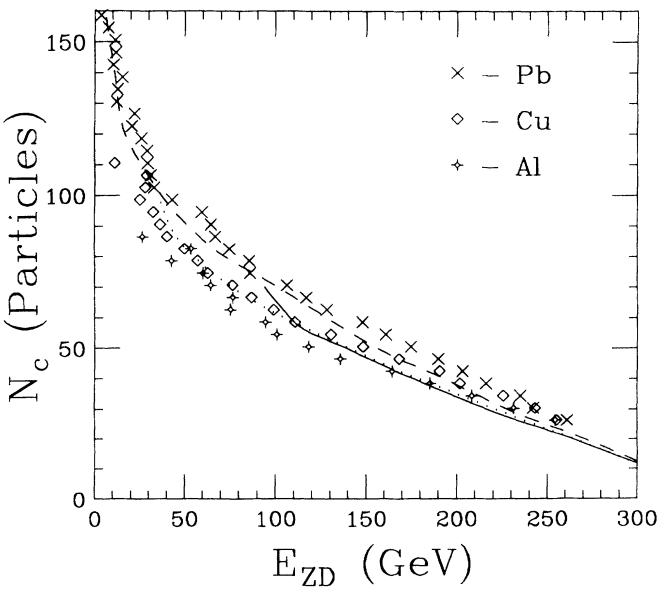

FIG. 2. The correlation between charged particle multiplicity and the zero degree energy measured by the E814 experiment for 14.6A GeV Si beams interacting with targets of Al, Cu, and Pb [37]. The curves (dash Pb, dot Cu, and solid Al) are the predictions of our model.

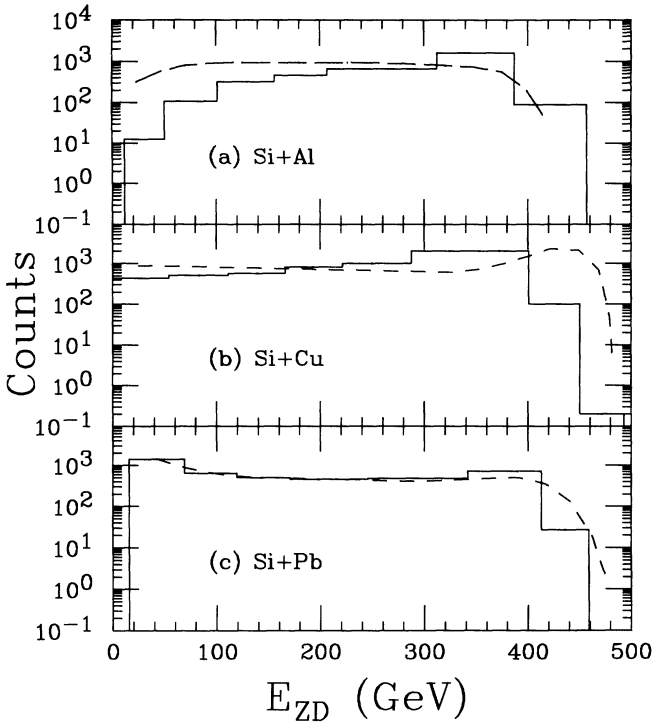

FIG. 3. The distributions of energy measured at zero degrees in interactions between Si nuclei, and targets of Al, Cu, and Pb. The solid lines are the data, and the dashed lines are the predictions of our model.

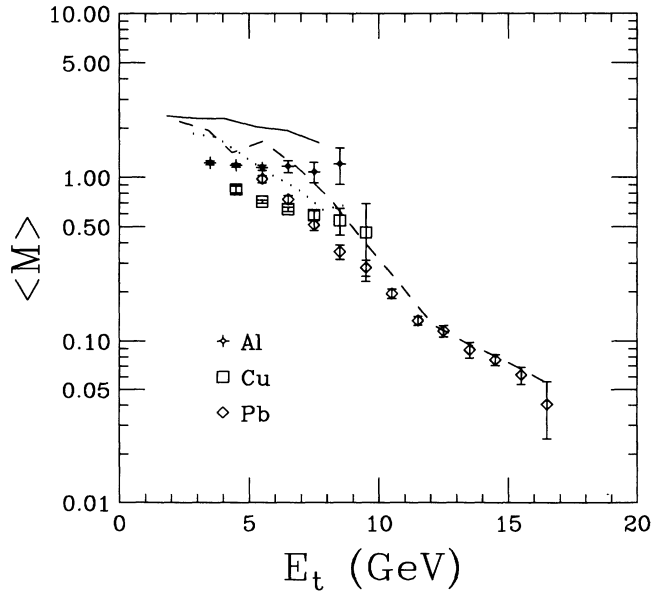

FIG. 4. The mean multiplicities per event $\langle M \rangle$ of beam rapidity particles measured by E814 plotted as a function of E_t [34,36]. The curves (dash Pb, dot Cu, and solid Al) are the predictions of the model under the assumption that the in-medium nucleon interaction cross section is 29 mb.

is able to describe the data at high values of E_t. It fails at low values since it does not distinguish between the presence of several nucleons in the final state, and the fact that some or several of these nucleons may be bound in clusters. The data shown are for protons only. The distributions for neutrons are similar. For the same number of interacted projectile nucleons, one expects to see more transverse energy generated in the heavier targets as a consequence of rescattering. In Fig. 4 one expects to see more E_t in the Pb target than in the Cu and Al targets, at the same value of $\langle M \rangle$. This is not seen in the data, but appears to be so in the calculation once one gets to moderate E_t for the Cu and Pb targets, when the effects of rescattering become important. It bears emphasis that the proton multiplicity at high E_t is rather sensitive to the choice of the in-medium nucleon interaction cross section. Hence calculations that use different cross sections [4,9,14] will differ on the number of nucleons they claim have interacted, and whose kinetic energy is available for antiproton production as is discussed below. Now that we have a means of determining the number of nucleons in the projectile that have interacted, we can examine how many antiprotons could be produced by these colliding nucleons.

III. ANTIPROTON PRODUCTION

At AGS energies, the production of antiprotons is very close to threshold ($\sqrt{s} - 4m_p < 1.5$ GeV). Hence it is reasonable to assume that antiprotons are made only in those collisons where the projectile and target nucleons are interacting for the first time. If either the projectile or target nucleon has been struck before, the energy available for particle production in subsequent collisions will in general be lower, and these interactions will be less likely to produce antiprotons. Figure 5 is a plot of the number of such first collisions, N_f, shown as a function of the number of projectile nucleons that have interacted, $N_{\rm int}$, for Si+Pb collisions. The ratio of the number of first collisions to the number of interacted nucleons is very close to 2. The geometrical dependence of antiproton production is then the same as the geometrical dependence of the number of first collisions. Table II shows the number of first collisions for various target projectile combinations. Also shown in the table are the results of calculations done by Costales [4] and Diebold [14]. The differences in the numbers come from differing choices in the in-medium cross section for the interaction of nucleons.

In our calculation, antiprotons are produced in the target at a rate commensurate with their estimated $p + p$ production multiplicity per collision [4,11], 1.2×10^{-3} at a beam energy of 14.6 GeV (actually, the measured $p+A$ value is $\sim 0.9 \times 10^{-3}$ per collision [13], and we estimate that the inclusion of Fermi motion in the projectile nucleus, and contributions from collisions other than the first, will raise this number by $\sim 25\%$). The shapes of the $\bar{p}$ rapidity distributions are chosen to be Gaussian with a width $\sigma_y = 0.5$ to be roughly consistent with the

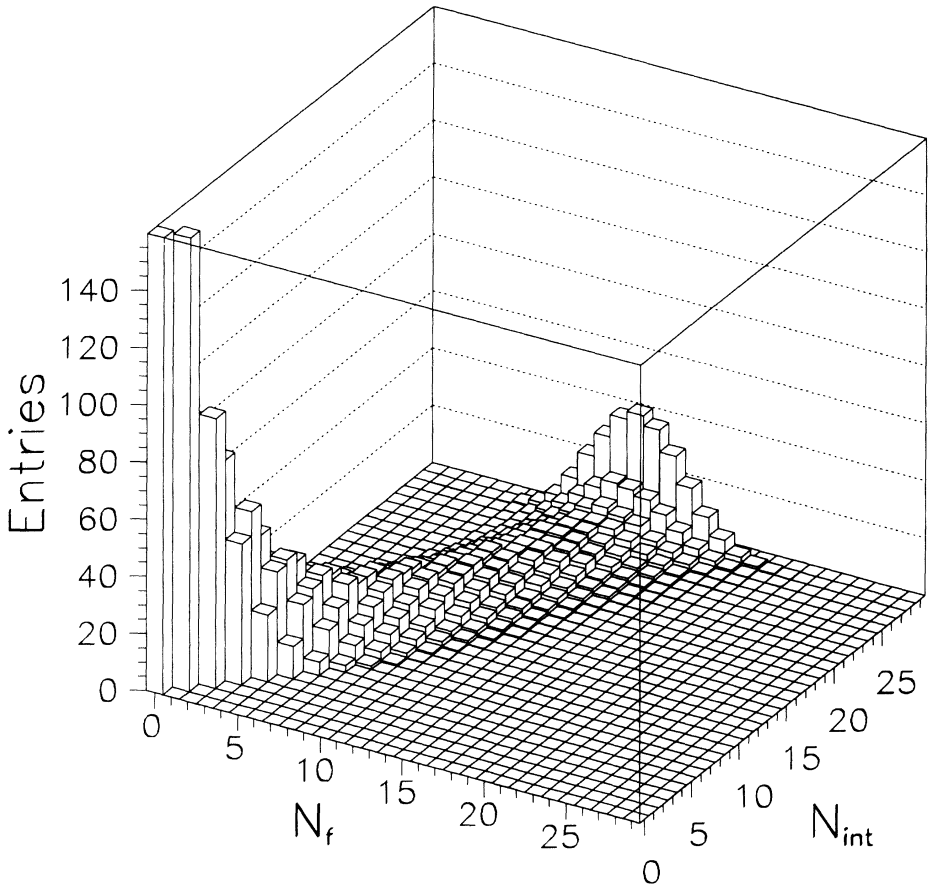

FIG. 5. The number of first collisions, N_f, plotted as a function of the number of projectile nucleons that have interacted, $N_{\rm int}$, in Si+Pb collisions.

measurements of experiment E858 at $p_t = 0$ [9]. The distributions transverse to the beam axis are chosen to be of the form

$$\frac{1}{p_t}\frac{dN}{dp_t dy} \propto e^{-m_t/B}, \tag{3}$$

TABLE II. The number of first collisions N_f calculated in several Glauber models of nucleus-nucleus collisions [4,14]. The numbers have been calculated for minimum bias and 7% most central collisions of Si and Au projectiles, with targets of Al, Cu, and Pb.

		N_f	
System and centrality	This work	Costales	Diebold
Si+Al			
Min. bias	3.4	3.6	
Central	9.1	8.8	
Si+Cu			
Min. bias	4.7		
Central	11.7		
Si+Au(Pb)			
Min. bias	6.4	6.3	6.0
Central	13.7	13.0	
Au+Au(Pt)			
Min. bias	17.1	14.0	12.0
Central	47.0	40.0	

where the transverse mass $m_t = \sqrt{m^2 + p_t^2}$, $m = 0.938$ GeV, and $B = 0.14$ or 0.2 GeV. The choice of B is motivated by preliminary analyses of data from experiments E802 and E859 [15]. The antiprotons are propagated through the target nucleus to see if they annihilate, with a cross section that is obtained from a fit to data [38]. The antiprotons can interact only after a formation time τ, which is varied in the calculation to show the effect of its choice on the results. At the same time, the antiprotons are also allowed to interact with the nucleons in the projectile. For these calculations, we assume that antiprotons are produced very early during the collision process, and that the environment they see is that of high baryon density in the projectile and target rapidities (i.e., the projectile and target nucleons remain at projectile and target rapidities, respectively). Such an assumption is quite reasonable for minumum bias collisions, and is the least applicable for central collisions. For central collisions, it is more appropriate to assume that the baryon density is maximal at center-of-mass rapidity. Also, we make the assumption that those antiprotons coming from the decay of $\bar{\Lambda}$ particles are created and annihilated in the same manner as the other antiprotons.

Figure 6 is a plot of the yield of antiprotons per event shown as a function of the number of projectile nucleons that have interacted in 14.6 GeV per nucleon Si + Al, Cu, and Pb collisions. The data are from experiment E814 [10]. The variable $N_{\rm int}$ was calculated as $28 - E_{ZD}/13.6$. The acceptance of the E814 apparatus for antiprotons was simulated using the code GEANT [39].

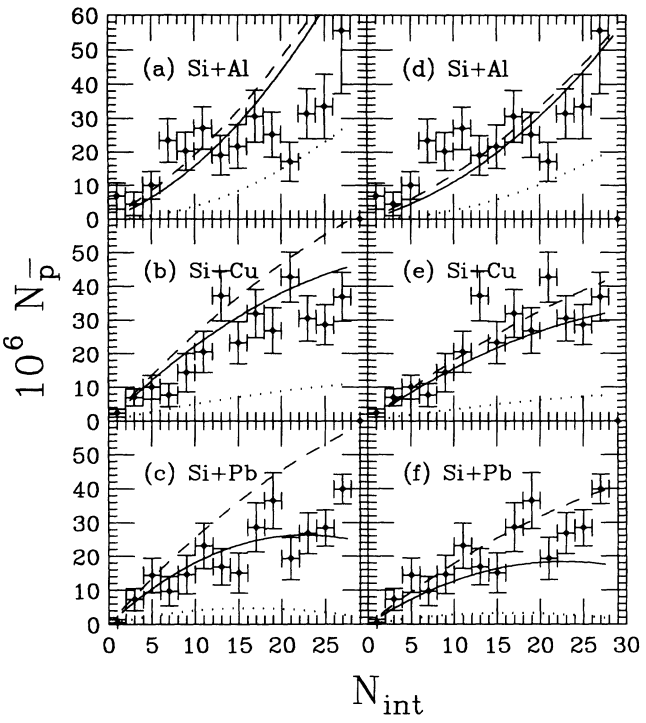

FIG. 6. The yield of antiprotons per event plotted as functions of the number of projectile nucleons that have interacted in collisions between Si nuclei, and targets of Al, Cu, and Pb. The data are from E814 [6,10]. The curves are the predictions of our model for $\bar{p}$ formation times τ equal to 1.5 (dot), 3.0 (solid), and 6.0 (dash). (a)–(c) use $B = 0.14$ GeV, and (d)–(f) use $B = 0.2$ GeV.

The model calculations have been corrected for this acceptance. The curves have been shown for three choices of formation time: 1.5, 3, and 6 fm/c. The first number implies that annihilation is allowed soon after the antiprotons are produced, and the last number essentially turns off annihilation. From the plot, one can see that in the calculation, the initial production of the antiprotons is similar for the three targets (see the $\tau = 6$ fm/c curve) for the same number of interacted nucleons. However, annihilation reduces the number of antiprotons (see curves for $\tau = 1.5$ fm/c) the most for the heaviest target. A favored value for τ is ~ 1.5 fm/c. The data, however, look similar for all three targets. This implies either that the production of antiprotons is enhanced relative to this calculation (as is modeled in RQMD [18]), or, that the annihilation of antiprotons is suppressed relative to these calculations (as is modeled by ARC [20]). Figures 6(a)–6(c) have been calculated with $B = 0.14$ GeV [4], in Eq. (3). On the basis of these plots, it was concluded [10] that if $\bar{p}$ production scaled with first collisions, then $\bar{p}$ annihilation was at the level of 40%. However, if instead of $B = 0.14$ we use $B = 0.2$ GeV [15], then we see from Figs. 6(d)–6(f) that the data would then be consistent with there being little or no annihilation relative to a first collision production, and the conclusions we would draw from the E802 data (discussed below) would be the same as from the E814 and E858 data.

Is it possible then to disentangle the effects of $\bar{p}$ production and annihilation? We believe this can be done by looking at the centrality and target dependence of the $\bar{p}$ rapidity (y) and transverse momentum (p_t) distributions, as is also discussed below.

There have been a few other attempts to study $\bar{p}$ production and annihilation in nucleus-nucleus collisons at AGS energies. In the first attempt, Costales [4] used simple parametrizations of $p + p$ data at 19 GeV to estimate the magnitudes and shapes of the distribution at an energy of 14.6 GeV. Such distributions were used in conjunction with a first collision model to describe the $\bar{p}$ data [11]. The calculations suggested that there was more $\bar{p}$ production than accounted for by first collision models. In a second calculation, Costales investigated $\bar{p}$ annihilation in a static participant volume [4]. The $\bar{p}$ survival was studied for a range of annihilation cross sections, with the conclusion that the data were consistent with minimal annihilation of the produced antiprotons. In a third calculation, under slightly different assumptions for the initial $\bar{p}$ yield, Costales concluded that $\bar{p}$ annihilation was at the level of 30% [4]. Antiproton annihilation was studied only in target matter.

In other work, $\bar{p}$ production at or close to $p_t = 0$ was estimated by parametrizing $\bar{p}$ production using the Feynmann scaling of $\bar{p}$ yields in $p + p$ collisions [9], or from data measured in $p + A$ collisions at several energies under kinematic conditions similar to the $A + A$ measurement [14]. The number of first collisions was calculated by Stankus in a model which assumed that the nucleus-nucleus inelastic cross section was 40 mb [9]. We expect his estimate for the number of first collisions to be similar to calculations done by Diebold subsequently [14] (see our Table II). Stankus concluded that $\bar{p}$ annihilation is minimal if the $\bar{p}$ yield scales with the number of first collisons. Diebold argues that if within a narrow kinematic range, the $\bar{p}$ yield is estimated from the first collisions scaling of $p + A$ data, the yields in $A + A$ collisions are rather well described. In such a prescription, one may be including some absorbtion expected to be present in the nuclear target used in the study of $p + A$ collisions [40]. No attempt was made by either Stankus or Diebold to investigate antiproton annihilation, or the impact parameter dependence of $\bar{p}$ production. A word of caution is in order about statements of whether or not the $\bar{p}$ distributions scale with the number of first collisions. The various authors define the number of first collisions in similar but not identical ways. Also, one must be careful to note what multiplicities for antiprotons are being assumed per first collision in the scaling procedure, and what kinematic regions are being studied. Further, the data are not in agreement as to whether the $\bar{p}$ yield increases or decreases in $p + p$ and $p + A$ collisions with increasing target mass [13,14]. Hence, while there is general agreement between the data, and the different calculations, it is not fruitful at this time to make an exhaustive study of the differences between the results of the calculations. The understanding of antiproton production will undoubtedly require the use of detailed models such as RQMD and ARC, and data measured with smaller statistical and systematic uncertainties.

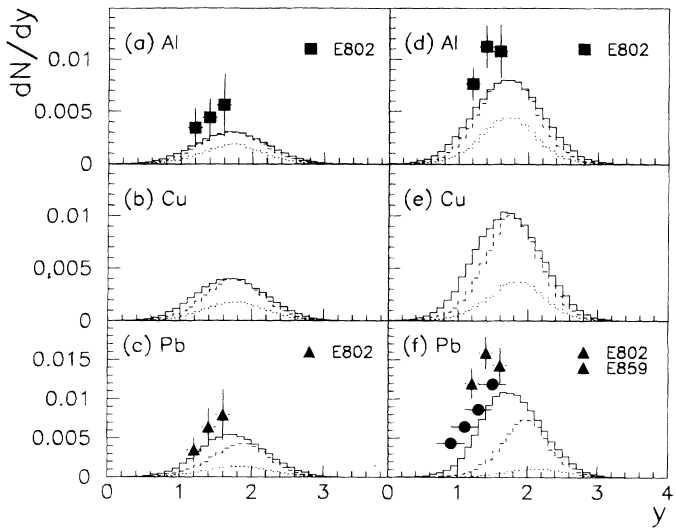

FIG. 7. The rapidity distributions of antiprotons calculated for (a)–(c) minimum-bias and (d)–(f) (7%) central Si+Al, Cu, and Pb interactions. The data are from E802 and E859 [4,11,15]. The curves are the predictions of our model for $\bar{p}$ formation times τ equal to 1.5 (dot), 3.0 (dash), and 6.0 (solid) fm/c.

Figure 7 shows the rapidity distributions of antiprotons calculated in our model for minimum bias, and (7%) central Si + Al, Cu, and Pb collisions. The data are from experiment E802 [11] and E859 [15] for Si+Al, Cu, and Au collisions. The calculations have been shown for three values of the formation time τ = 1.5, 3.0, and 6.0 fm/c. The antiprotons were produced only in first collisions. Once again, the model is able to describe the data if the formation time is assumed to be $\sim$ 6.0 fm/c. If $\bar{p}$ production were enhanced by multiple collisions, the data might be better described using a smaller formation time and hence larger absorption. It is interesting to note that the rapidity distribution shifts upwards in rapidity for the heaviest target if absorption is large. Such effects are even observable in minimum bias collisions, and are rather pronounced in central collisions. The data do not cover a sufficiently wide range in rapidity to infer whether the mean of the rapidity distribution is varying with centrality. Experiment E878 has measured the rapidity distributions of antiprotons at p_t = 0 as functions of centrality, and it would be interesting to see how the location of the peak of the rapidity distribution depends on centrality [16]. As mentioned previously, our model assumes a rapidity distribution for nucleons which is incorrect in small impact parameter collisions. In comparison to the model, there will be more baryons at mid

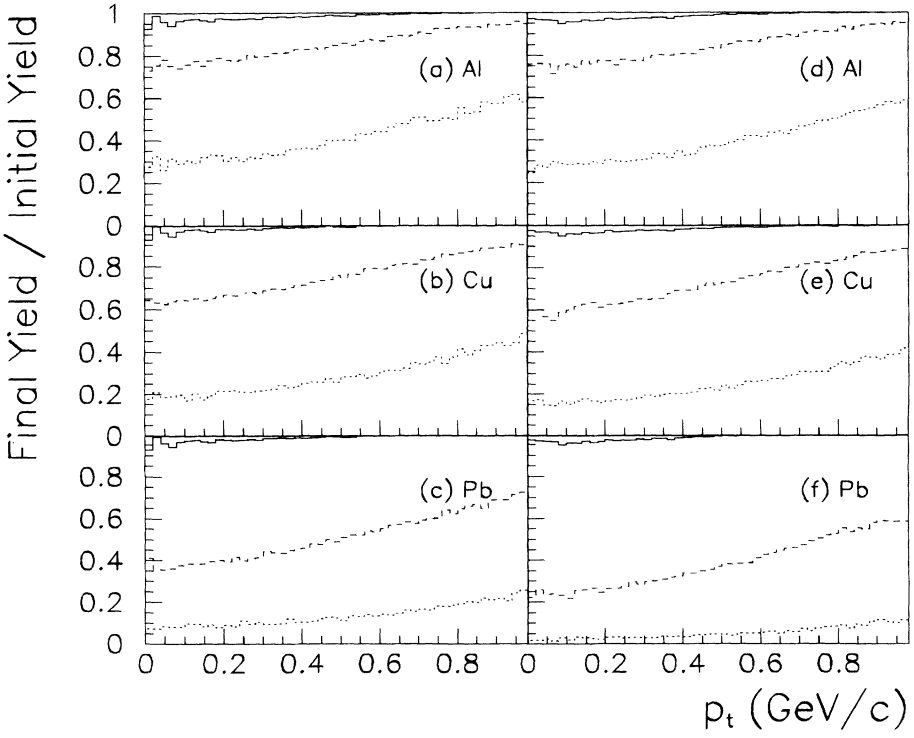

FIG. 8. The ratio of the number of antiprotons surviving annihilation to the number produced in (a)–(c) mimimum bias and (d)–(f) central interactions of Si beams and targets of Al, Cu, and Pb. The curves are the predictions of our model for $\bar{p}$ formation times τ equal to 1.5 (dot), 3.0 (dash), and 6.0 (solid) fm/c.

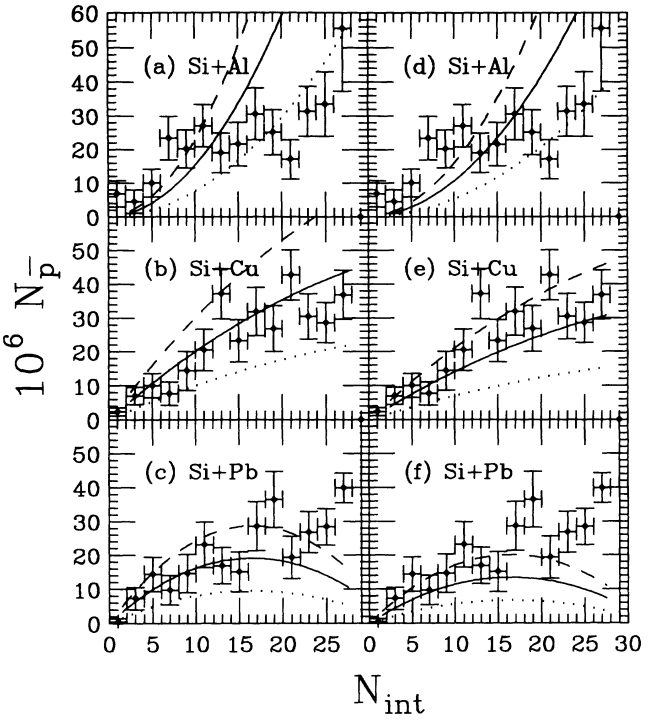

FIG. 9. The yield of antiprotons per event plotted as functions of the number of projectile nucleons that have interacted in collisions between Si nuclei, and targets of Al, Cu, and Pb. The data are from E814 [6,10]. The curves are the predictions of our model for a $\bar{p}$ formation time $\tau = 1.5$ fm/c. The $\bar{p}$ production enhancement factors are 2.0 (dots), 4.0 (solid), and 6.0 (dash) relative to a first collision model. (a)–(c) use $B = 0.14$ GeV, and (d)–(f) use $B = 0.2$ GeV.

rapidity, and these will tend to produce a less pronounced rapidity shift of the $\bar{p}$ spectrum in central Si+Pb collisions. However, there will be increased $\bar{p}$ absorption at central rapidity, and this will result in an increase in the width of the $\bar{p}$ distribution as was reported for Au+Au collisions by the E878 experiment [17].

Figure 8 shows the results of our calculation of the ratio of the number of surviving antiprotons to the initial number of antiprotons produced, plotted as a function of p_t (integrated over all rapidity) for minimum bias and central Si+ Al, Cu, and Pb collisions. As before, the curves are shown for the formation times 1.5, 3.0, and 6.0 fm/c. There is a clear suppression of antiprotons at low p_t on account of absorption. The effect is larger for central Si+Pb collisions, and is expected to be larger still in central Au+Au collisions. The p_t distribution of antiprotons has been studied elsewhere in the context of differences expected in the propagation of protons and antiprotons through dense nuclear matter [41]. It was argued there that the mean field would reduce the effective temperature of the antiproton spectrum. The effect of absorption was also discussed. The absorption of antiprotons at low p_t would increase the effective temperature of the $\bar{p}$ spectrum. Once again, it would be interesting to look for such effects at central rapidity in $\bar{p}$ distributions studied as functions of centrality. Such data should become available from the E864 experiment in the coming year.

We now discuss briefly what our model would predict if $\bar{p}$ production were enhanced in our calculations relative to a first collision model. Figure 9 shows the yields of antiprotons as in Fig. 6. The predictions are shown for a formation time $\tau = 1.5$ fm/c. Figures 9(a)–9(c) are for $B = 0.14$ GeV and Figs. 9(d)–9(f) are for $B = 0.2$ GeV. The three curves are for $\bar{p}$ production enhanced relative to the corresponding $\tau = 1.5$ fm/c curve in Fig. 6 by factors of 2, 4, and 6, respectively. The enhancement factors were chosen to be roughly consistent with the extent of enhanced $\bar{p}$ production claimed in the RQMD model. One can see from the figure that while factors of 2 and 4 enhancement followed by large annihilation ($\tau = 1.5$ fm/c) would be consistent with the Si+Al and Si+Cu data, respectively, the shapes of the predictions for Si+Pb collisions differ from the data.

Figure 10 is similar to Fig. 7. In this figure, we have enhanced the production of antiprotons in the calculation by factors of 2, 4, and 6 for Si+Al, Cu, and Pb interactions, respectively. The curves are now shown for

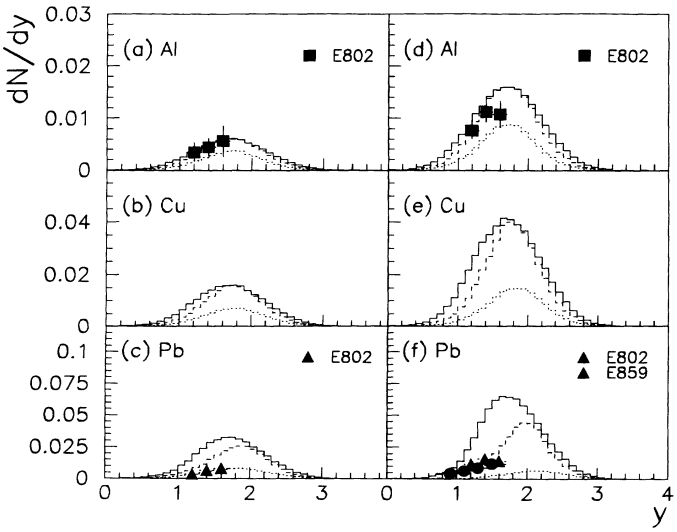

FIG. 10. The rapidity distributions of antiprotons calculated for (a)–(c) minimum-bias and (d)–(f) central Si+Al, Cu, and Pb interactions. The data are from E802 and E859 [4,11,15] for Si+Al and Au interactions. The curves are the predictions of our model for $\bar{p}$ formation times τ equal to 1.5 (dot), 3.0 (dash), and 6.0 (solid) fm/c. The $\bar{p}$ enhancement factors are 2, 4, and 6 for Si+Al, Cu, and Pb collisions, respectively.

formation times $\tau = 1.5$, 3.0, and 6.0 fm/c. We note that a fixed enhancement factor is not able to describe both minimum bias, and central collision data, indicating that in the presence of large $\bar{p}$ absorption, $\bar{p}$ production is more enhanced in central collisions relative to our calculation.

IV. SUMMARY AND CONCLUSIONS

We have developed a simple model to describe several of the features seen in the data of experiments E814 and E802. We have used the model to highlight the degree to which the E_t and N_c distributions are determined by collision geometry. The model was then applied to describe the centrality dependence of $\bar{p}$ production measured by E814. We found that the bulk of the available experimental data on antiprotons produced in nucleus-nucleus collisions are consistent with a scenario in which the $\bar{p}$ yield increases linearly with the number of first collisions if there is minimal annihilation of the produced antiprotons. An alternative scenario supported to some degree by our calculations is that enhanced $\bar{p}$ production is followed by large annihilation This latter scenario does not describe the data as well the former. We are looking forward to the availability of more data and better calculations to understand the mechanisms by which antiprotons are produced and annihilated in nucleus-nucleus collisions.

ACKNOWLEDGMENTS

This work was supported in part by Grant No. DE-FG02-91ER-40609 with the U.S. Department of Energy. We thank J. Costales for useful discussions.

[1] Quark Matter '93 [Nucl. Phys. **A566**, 1 (1994)].
[2] T.A. DeGrand, Phys. Rev. D **30**, 2001 (1984); C.M. Ko and X. Ge, Phys. Lett. B **205**, 195 (1988); D.H. Rischke *et al.*, Phys. Rev. D **41**, 111 (1990).
[3] S. Gavin, M. Gyulassy, M. Plumer, and R. Venugopalan, Phys. Lett. B **234**, 175 (1990).
[4] J. Costales, Ph.D. thesis, Massachusetts Institute of Technology, 1991.
[5] E814 Collaboration, S.V. Greene *et al.*, Nucl. Phys. **A544**, 599c (1992).
[6] S.V. Greene, Ph.D. thesis, Yale University, 1992.
[7] E858 Collaboration, P. Stankus *et al.*, Nucl. Phys. **A544**, 59c (1992).
[8] E858 Collaboration, P. Stankus *et al.*, in "Heavy Ion Physics at the AGS," edited by S.G. Steadman, W.L. Kehoe, and G.S.F. Stephans, MIT Report No. MITLNS-2158, 1993 (unpublished), p. 134.
[9] P. Stankus, Ph.D. thesis, Columbia University, 1993 (unpublished).
[10] E814 Collaboration, J. Barrette *et al.*, Phys. Rev. Lett. **70**, 1763 (1993).
[11] E802 Collaboration, A. Abbott *et al.*, Phys. Lett. B **271**, 447 (1991).
[12] E858 Collaboration, A. Aoki *et al.*, Phys. Rev. Lett. **69**, 2345 (1992).
[13] E802 Collaboration, A. Abbott *et al.*, Phys. Rev. C **70**, 1393 (1993).
[14] E886 Collaboration, G. Diebold *et al.*, Phys. Rev. C **48**, 2984 (1993).
[15] P. Rothschild, Ph.D. thesis, Massachusetts Institute of Technology, 1994 (unpublished); P. Rothschild *et al.*, in "Heavy Ion Physics at the AGS" [8], p. 153; E859 Collaboration, G.S.F. Stephans *et al.*, Nucl. Phys. **A566**, 269c (1994).
[16] E878 Collaboration, M. Bennett (private communication).
[17] E878 Collaboration, B. Shiva Kumar *et al.*, Nucl. Phys. **A566**, 439c (1994).
[18] A. Jahns, H. Stöcker, W. Greiner, and H. Sorge, Phys. Rev. Lett. **68**, 2895 (1992).
[19] A. Jahns, in "Heavy Ion Physics at the AGS" [8], p. 120.
[20] Y. Pang, T. Schlagel, S. Kahana, and C. Dover, Phys. Rev. C **47**, 1356 (1993).
[21] S. Kahana, in "Heavy Ion Physics at the AGS" [8], p. 263.
[22] T. Schlagel, S. H. Kahana, and Y. Pang, Phys. Rev. Lett. **69**, 1290 (1992).
[23] K. Werner, Z. Phys. C **42**, 85 (1989).
[24] A. Shor and R. Longacre, Phys. Lett. B **218**, 100 (1989).
[25] B. Andersson *et al.*, Phys. Rep. **97**, 31 (1983); Nucl. Phys. **B281**, 289 (1987).
[26] H. Sorge, H. Stöcker, and W. Greiner, Ann. Phys. (N.Y.) **191**, 266 (1989).
[27] Y.J. Pang, T.J. Schlagel, and S.H. Kahana, Phys. Rev. Lett. **68**, 2743 (1992).
[28] D.J. Dean, A.S. Umar, and M. Strayer, Phys. Rev. C **48**, 2433 (1993).
[29] A.J. Baltz, Nucl. Phys. **A525**, 639c (1991); Phys. Rev. C **43**, 1420 (1991).
[30] R. Shanta and S.K. Gupta, Z. Phys. A **338**, 183 (1991).
[31] G. Baym, V. Ruuskanen, and P. Braun-Munzinger, Phys. Lett. B **190**, 29 (1987).
[32] M.J. Tannenbaum, Int. J. Mod. Phys. A **4**, 3377 (1989).
[33] B. Shiva Kumar, in "Heavy Ion Physics at the AGS," edited by O. Hansen, Brookhaven National Laboratory Report No. BNL-44911, 1990 (unpublished).
[34] E814 Collaboration, J. Barrette *et al.*, Phys. Rev. Lett. **64**, 1219 (1990).
[35] E814 Collaboration, J. Barrette *et al.*, Phys. Rev. C **45**, 819 (1992).
[36] J.T. Mitchell, Ph.D. thesis, Yale University, 1992.
[37] E814 Collaboration, J. Barrette *et al.*, Phys. Rev. C **46**, 312 (1992).
[38] P. Koch and C. Dover, Phys. Rev. C **40**, 145 (1989).
[39] R. Brun *et al.*, GEANT, version 3.14, CERN Data Handling Division, Report No. DD/EE/84-1 (unpublished).
[40] A. Jahns, C. Spieles, R. Mattiello, H. Stöcker, W. Greiner, and H. Sorge, Phys. Lett. B **308**, 11 (1993).
[41] V. Koch, G.E. Brown, and C.M. Ko, Phys. Lett. B **265**, 29 (1991).